A STUDY OF LAMINAR FLOW OVER THE BRAZILIAN SATELLITE LAUNCH VEHICLE USING THE CHIMERA TECHNIQUE

Leonor Camila Q. Yagua – camila@aer.ita.cta.br
Centro Técnico Aeroespacial, Instituto Tecnológico de Aeronáutica
CTA/ITA/IEA – 12228-900 – São José dos Campos, SP, Brasil
João Luiz F. Azevedo – azevedo@iae.cta.br
Centro Técnico Aeroespacial, Instituto de Aeronáutica e Espaço
CTA/IAE/ASE-N – 12228-904 – São José dos Campos, SP, Brasil

Abstract. *This work presents numerical simulations of the flow over the first Brazilian satellite launch vehicle, VLS. The algorithm solves the thin-layer Navier-Stokes equations for compressible flows using the Chimera technique. The computational code considers a finite difference formulation and the time discretization uses an explicit method. The spatial discretization uses a centered scheme in which the artificial dissipation terms are explicitly added. Pressure coefficient results obtained in the present simulations are compared to experimental data.*

Keywords: *CFD, VLS, Multiblock Grids, Numerical Simulation, Chimera Technique.*

1. INTRODUCTION

The overlapping multiblock grid technique, Chimera, became a practical method for obtaining solutions in different types of problems. One can work with simple and complex configurations, and with compressible (Rock & Habchi,1998) and incompressible flows (Chattot & Wang, 1998). This technique allows the use of simple computational grids over each component of the geometry in order to form a composite mesh which allows the discretization of complex configurations.

The computational code developed in the context of the present work solves the 3-D thin-layer Navier-Stokes equations, and it considers the formulation in the conservative form. The Chimera technique is described in detail in Section 3. This technique typically discretizes each component of a complex configuration with its own grid block. When all grid blocks are joined together in order to create the composite mesh, clearly there will exist regions of overlap among the various grid blocks. Hence, in order to create the final composite grid and to generate all the geometric information necessary to actually run a Chimera simulation, two steps must be considered: the hole cutting process and the interpolation process. The hole-cutting process

consists in the elimination of the points of one grid block which lie inside the components of another grid block or the elimination of points in regions of excessive grid overlap. In the hole-cutting process, the points in the hole, the hole boundary points and their neighboring points in the other grid block are defined. These neighboring points are used in the interpolation process, since the values of the properties of the hole boundary points are obtained by interpolation using exactly the properties of this neighboring points in the other grid block. The interpolation process clearly has to be performed at each time step of the overall solution algorithm. However, all the weights used in this process can be computed *a priori* and stored. In its present version, the code uses trilinear interpolation for the update of the properties along the hole boundary.

The purpose of this work is to study the issues which can appear in the actual implementation for a truly complex configuration. The simulations to be considered here emphasize flow calculations over the VLS. Since only zero angle-of-attack cases are considered in the present work, the flow over the complete VLS vehicle will have a double symmetry. In this condition, one can work with a simplified configuration of the VLS, treating only a quarter of the central body and one booster. This saves computational time and, therefore, it is the solution adopted here. Axisymmetric calculations were performed for the VLS central body configuration by Buonomo, Strauss & Azevedo (1998), and a preliminary 2-D analysis with the Chimera technique for the VLS at zero angle-of-attack is discussed in Yagua, Basso & Azevedo (1999). The present work intends to extend the capability of computing VLS flows in order to include a 3-D viscous formulation. The work considers supersonic flow conditions over the VLS and the present numerical results are compared to experimental data.

2. THEORETICAL FORMULATION

The compressible thin-layer Navier-Stokes equations can be written in conservative form for three dimensional, general curvilinear coordinates as

$$\frac{\partial \hat{Q}}{\partial \tau} + \frac{\partial \hat{E}}{\partial \xi} + \frac{\partial \hat{F}}{\partial \eta} + \frac{\partial \hat{G}}{\partial \zeta} = \text{Re}^{-1} \frac{\partial \hat{S}}{\partial \eta}, \tag{1}$$

where *Re* is the Reynolds number and $\hat{Q}$ is the vector of conserved variables defined by

$$\hat{Q} = \begin{bmatrix} \rho & \rho u & \rho v & \rho w & e \end{bmatrix}^t \tag{2}$$

and $\hat{E}, \hat{F}$ and $\hat{G}$ are the inviscid flux vectors. These can be defined as

$$\hat{E} = J^{-1} \begin{Bmatrix} \rho U \\ \rho u U + \xi_x p \\ \rho v U + \xi_y p \\ \rho w U + \xi_z p \\ U(e+p) - \xi_t p \end{Bmatrix}, \hat{F} = J^{-1} \begin{Bmatrix} \rho V \\ \rho u V + \eta_x p \\ \rho v V + \eta_y p \\ \rho w V + \eta_z p \\ V(e+p) - \eta_t p \end{Bmatrix}, \hat{G} = J^{-1} \begin{Bmatrix} \rho W \\ \rho u W + \zeta_x p \\ \rho v W + \zeta_y p \\ \rho w W + \zeta_z p \\ W(e+p) - \zeta_t p \end{Bmatrix}. \tag{3}$$

The thin-layer viscous flux vector, $\hat{S}$, can be represented as

$$\hat{S} \;=\; J^{-1}\begin{Bmatrix} 0 \\ \mu\,m_1 u_\eta + (\mu/3)m_2\eta_x \\ \mu\,m_1 v_\eta + (\mu/3)m_2\eta_y \\ \mu\,m_1 w_\eta + (\mu/3)m_2\eta_z \\ \mu\,m_1 m_3 + (\mu/3)m_2(\eta_x u + \eta_y v + \eta_z w) \end{Bmatrix}, \tag{4}$$

where

$$\begin{aligned}
m_1 &= \eta_x^2 + \eta_y^2 + \eta_z^2 \,, \\
m_2 &= \eta_x u_\eta + \eta_y v_\eta + \eta_z w_\eta \,, \\
m_3 &= (u^2 + v^2 + w^2)_\eta/2 + \Pr^{-1}(\gamma-1)^{-1}(a^2)_\eta \,,
\end{aligned} \tag{5}$$

and only the thin-layer terms (Pulliam, 1980) have been included in the previous expressions. The formulation assumes that η is the wall-normal direction. The metric terms used and the Jacobian are also defined in Yagua & Azevedo (1999). The contravariant velocity components can be represented as

$$\begin{aligned}
U &= \xi_t + \xi_x u + \xi_y v + \xi_z w \,, \\
V &= \eta_t + \eta_x u + \eta_y v + \eta_z w \,, \\
W &= \zeta_t + \zeta_x u + \zeta_y v + \zeta_z w \,.
\end{aligned} \tag{6}$$

The governing equations are discretized in a finite difference fashion. Space discretization uses central differences together with explicit added artificial dissipation terms. Time march uses the explicit Euler method, for simplicity of implementation at this point. The equations, after both space and time discretization, can be written in operator form as

$$\Delta\hat{Q}^n \;=\; R_\xi + R_\eta + R_\zeta \tag{7}$$

The operators used in the Eq. (7) can be expressed by

$$\begin{aligned}
R_\xi &= -\Delta t\,\delta_\xi\,\hat{E}^n + D_\xi \,, \\
R_\eta &= -\Delta t\,\delta_\eta\,\hat{F}^n + D_\eta \,, \\
R_\zeta &= -\Delta t\,\delta_\zeta\,\hat{G}^n + D_\zeta \,.
\end{aligned} \tag{9}$$

The D_ξ, D_η and D_ζ operators are 5-point, central difference operators in the ξ, η and ζ directions, respectively. The artificial dissipation terms used, i.e., D_ξ, D_η and D_ζ are inspired on Pulliam's linear artificial dissipation operators (Pulliam, 1986). These use a 5-point stencil in order to obtain 4th-difference dissipation operators. The actual form of the operators used in the present work is

$$D_\xi = -\Delta t \varepsilon_E J^{-1} \psi_\xi \left(\nabla_\xi \Delta_\xi \right)^2 J \overline{Q}^n,$$

$$D_\eta = -\Delta t \varepsilon_E J^{-1} \psi_\eta \left(\nabla_\eta \Delta_\eta \right)^2 J \overline{Q}^n, \qquad (10)$$

$$D_\zeta = -\Delta t \varepsilon_E J^{-1} \psi_\zeta \left(\nabla_\zeta \Delta_\zeta \right)^2 J \overline{Q}^n,$$

where the ψ_ξ, ψ_η and ψ_ζ coefficients are defined as

$$\psi_\xi = \left| \xi_x \right| + \left| \xi_y \right| + \left| \xi_z \right|,$$

$$\psi_\eta = \left| \eta_x \right| + \left| \eta_y \right| + \left| \eta_z \right|, \qquad (11)$$

$$\psi_\zeta = \left| \zeta_x \right| + \left| \zeta_y \right| + \left| \zeta_z \right|.$$

These coefficients were introduced by Benek, Buning and Steger (1985) in order to improve the convergence rate of the overall algorithm.

3. CHIMERA TECHNIQUE

The Chimera technique can use many structured grids which are created independently. Every grid is created for a specified part of a complex configuration and these are later joined together in order to cover the complete geometry. Generally, this technique considers a main grid about the overall configurations with smaller and simpler grids embedded in areas of interest. Each grid is operated independently by the solver and they communicate through overlapped boundary regions. This technique has two steps, the hole cutting process and the interpolation process which are described subsequently.

3.1 Hole Cutting

One can observe that, after the independently created grids are joined together, many overlapped regions appear. It is necessary to identify which mesh is the main grid and which meshes are the secondary grids. Afterwards, holes have to be created in the main grid in order to accommodate for the secondary grids. Some overlapped regions also contain points inside some of the other components of the geometry. These points have to be eliminated. The elimination of the points is performed considering two arrays, $iblanck_m$ (i,j,k) and $nfront_m$ (i,j,k), for every (i,j,k) point and for each m-th block. One can assume as initial values $iblanck_m$ $(i,j,k) = 1$ and $nfront_m$ $(i,j,k) = 0$. The $iblanck_m$ (i,j,k) array informs which points are inside or outside the hole, and $nfront_m$ (i,j,k) gives the information about the neighboring points.

The points which are considered inside the hole are the points which are inside the boundary surface. This boundary surface could be defined through a flag variable j_{ref}. If $j_{ref} = 1$, the hole will be created only for the geometry. With the purpose of obtaining a larger hole, the j_{ref} variable will be greater than 1. If the (i,j,k) point is inside the hole then $iblanck_m$ (i,j,k) is zero. Otherwise, it is one. If the (i,j,k) point is inside the geometry, the $iblanck_m$ (i,j,k) is also zero. The value of the $nfront_m$ (i,j,k) array is set to one, if the (i,j,k) point is a boundary surface point.

For every point in which $nfront_m$ $(i,j,k)=1$, it is necessary to look for and identify which points in the other grid are neighboring points. At the end of this process, the boundary points

and the their respective neighboring points are identified and stored in a matrix to be used by the interpolation procedure.

3.2 Interpolation

The communication between the grids is performed through interpolation of overlapped boundary values from the grid which contained the overlapped region. This overlapped boundary is the boundary of the hole in the main grid case and the external boundary for the secondary grids. In the present approach, the secondary grids have all of their boundary points immersed in the main grid. Hence, the properties for these points must be interpolated. In this process, one can readily obtain the points which are in the overlapped boundary due to the hole cutting process, since they have been already identified and stored.

The property values of the internal boundary points are obtained through interpolation of the properties from the neighboring points in the other mesh. In this process, it is necessary to calculate the distance between the hole boundary points and its neighboring points. The distance information will be used as weighting factor in the actual interpolation formulas. In this work, the implementation uses a trilinear interpolation. Hence, property values at the overlapped boundary points are obtained by weighted averages which take into account the distance between the boundary point and the neighboring points in the other meshes. Finally, when one has the necessary information to calculate the properties in the overlapped region, it is possible to update the properties in the boundary points with the current value of this information. The overlapped boundary points do not enter in the solution algorithm. In the flow solver, one can consider $\Delta\hat{Q}\ (i,j,k) = 0$ for every point which is inside the hole.

4   RESULTS

This section describes the physical problem, grid generation and the numerical results. It also presents the comparison of these computational results with experimental data.

4.1 Physical Problem

The VLS vehicle consists of one central body and four boosters. The distance between the booster and the central body is only about 10% of the diameter of the main body. The wall boundary conditions are implemented considering the no slip condition. The Reynolds number used here is 20 X 10^6 and the freestream Mach number is $M_\infty = 2.0$. The simulations consider a zero angle-of-attack case.

4.2   Grid Generation

As previously discussed, the complete configuration consists in one central body and four boosters (Fig. 1). However, due to symmetry considerations for zero angle-of-attack flows, the simulation can consider only one-quarter of the central body and one booster. Therefore, it is possible to create a grid with only two blocks, i.e., a grid block for the central body and another one for the booster. Both grids were created by an algebraic generator (Fletcher, 1990). The central body grid has 80 points in the ξ direction, 40 points in the η direction and 13 points in the

ζ direction. Similarly, the booster grid was created considering 60 points in the ξ direction, 40 points in the η direction and 19 points in the ζ direction (Fig. 2).
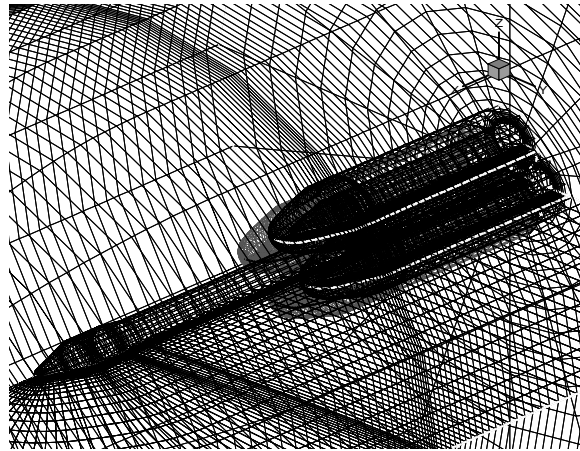
Figure 1- View of the complete VLS grid.
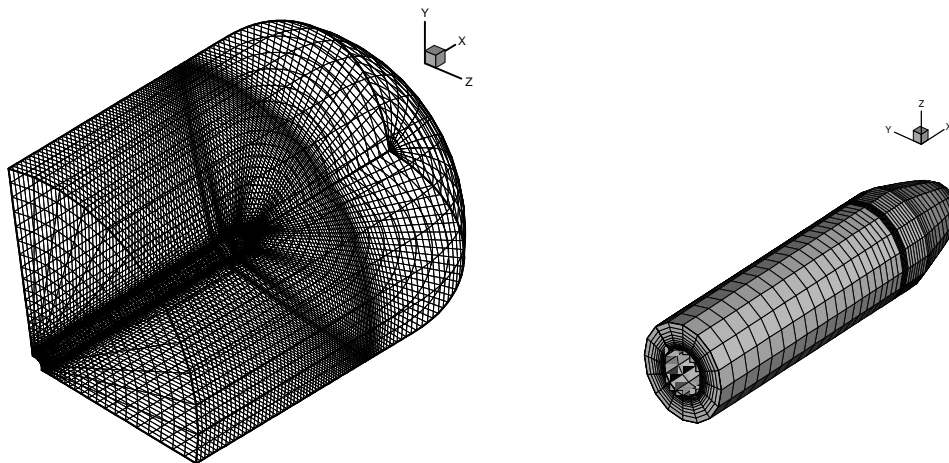
Figure 2-View of the VLS central core grid and booster grids.

One can appreciated the overlapping region for this problem in Fig. 3. The points of the VLS grid which are inside of the booster are eliminated. After the hole cutting process, one can obtain the hole made in the VLS grid. Even though the hole cutting procedure was performed on different central body grid planes, one can observed it in one of these planes in Fig. 4. The dark region represents the hole in this figure.

4.3 Numerical Results

The results obtained with the thin-layer Navier-Stokes formulation are shown in Figs. 5-7. One can observe pressure contours in the wall of the VLS central body and along the booster wall in Fig. 5. Both configurations achieve the maximum pressure at the nose of bodies, as one should expect. With the purpose of facilitating the visualization of the results, some figures show the results in a plane of the VLS grid which is orthogonal to the booster configuration. The Mach number contours are shown in Fig. 6. A strong shock is captured in the nose region. Much of the

detail of the aerodynamic features near the booster nose cannot be seen in Fig. 6. However, it is clear from this figure that a strong, detached shock wave is also being captured by simulation.
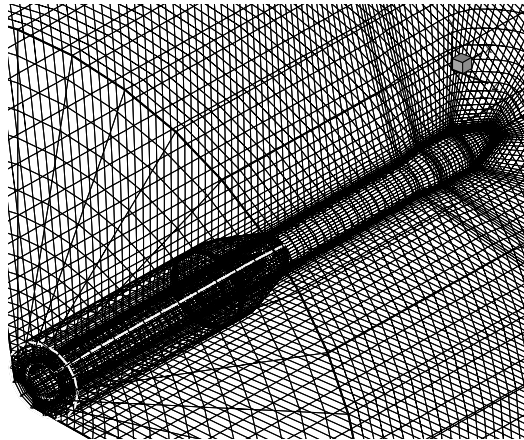
Figure 3-Overlapping region between VLS central body grid and booster grids.
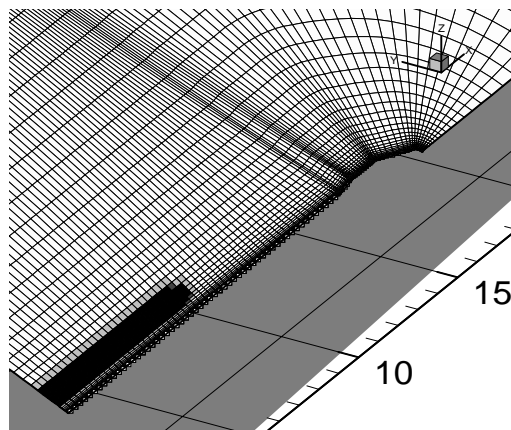
Figure 4-The VLS central body grid with the hole in one plane.
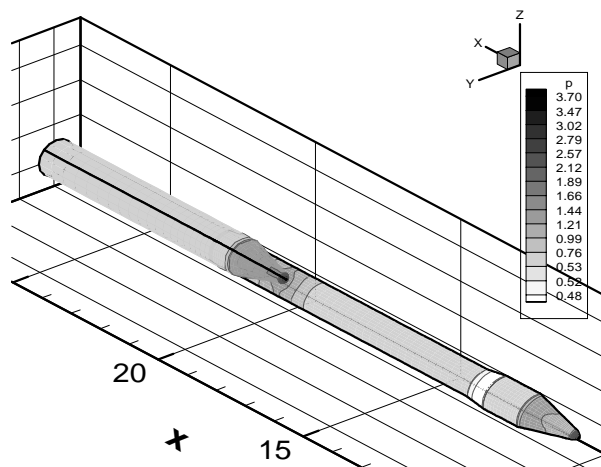
Figure 5-Pressure contours along the VLS main body and booster walls for $M_\infty = 2$ and $\propto=0$ deg.

The velocity vector field near the booster nose can be seen in Fig. 7. This figure actually shows two different results. The figure to the left, case (a), presents the velocity vectors when the central body mesh has 80 points in the ξ direction. Similarly, the figure to the right, case (b), has results for the velocity vector field when the central body grid has 100 points in the ξ direction. All the other parameters are unchanged between the two calculations which are shown in Fig. 7. Pressure contours in the field in the vicinity of the booster nose can be seen in Fig. 8. In this case, the central body mesh with 100 points in the ξ direction is used for the computations.
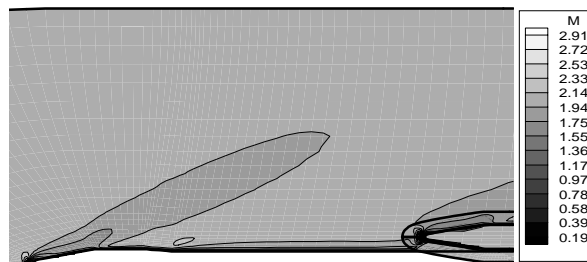
Figure 6-Mach number contours for a longitudinal plane including the central body and booster for $M_\infty = 2$ and $\propto=0$ deg.
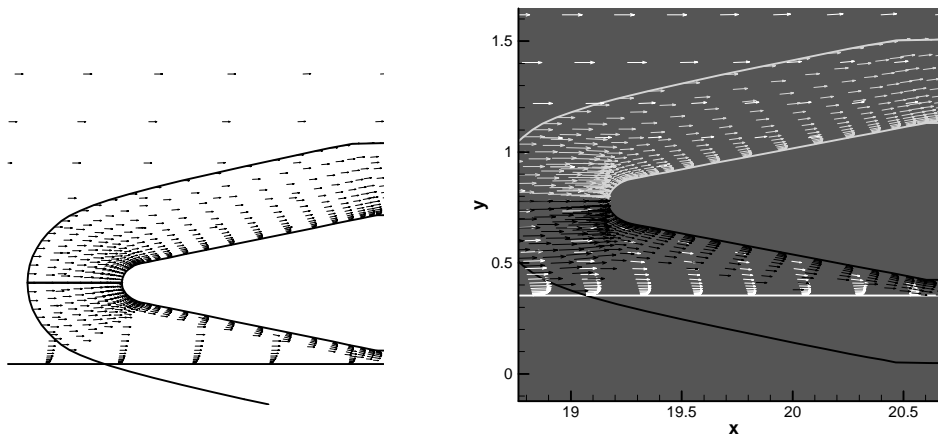
Figure 7-Velocity vector field in the overlapping region. Central body grid has: (a) 80 x 40 x 13 points; (b) 100 x 40 x 13 points.

The comparison between numerical and experimental results is indicated in Fig. 9. In this case, pressure coefficient distributions along the central body wall, for an azimuthal plane which contains the booster axis, are presented for the two different computational grids previously described. The left graph has the results for the case in which the central body grid has 80 x 40 x 13 points, whereas the right graph has the results for the 100 x 40 x 13 point grid. In both cases, the booster grid has 60 x 19 x 17 points. Both comparisons indicate that the agreement in the forward portions of the vehicle is very good. In the downstream portion of the vehicle, and

especially in the region in which there is a close interaction between central body and booster flows, the agreement between computation and experiments is not as good. Nevertheless, one can already observe a considerable improvement in the Cp correlation in the first booster bow shock reflection region with the finer grid calculation. Therefore, at this point along the present development effort, it is expected that further grid refinement in this interaction region would further improve the correlation between computational and experimental results. It should be also observed that the booster grid in the overlapped region is still finer than the fine central body grid in the same region. Hence, this is another aspect that could be affecting the quality of the solution in the interaction region.
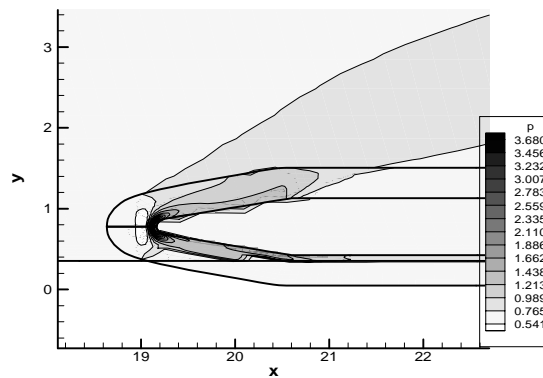
Figure 8-Pressure contours in the overlapping region for the central body grid with 100 x 40 x 13 points.
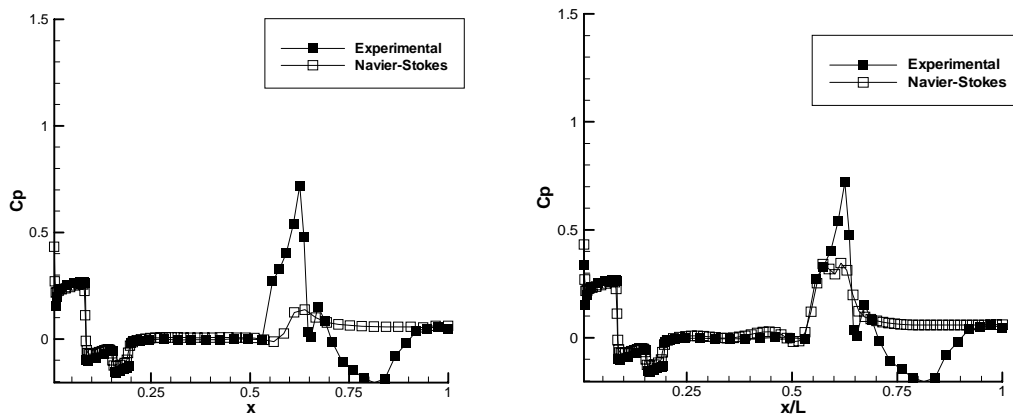
Figure 9 –Comparison of Cp between numerical and experimental results in the wall of the VLS central body for $M_\infty = 2$ and $\propto = 0$ deg. Central body grid has: (a) 80 points in the ξ direction; (b)100 points in the ξ direction.

5 CONCLUSION

The paper presents 3-D compressible flow results for Chimera grid simulations over the first Brazilian Satellite launcher. The 3-D code is an extension of previously validated 2-D solvers and

the present calculations seem to indicated that the extension process was adequately performed. Furthermore, continuity of the contour lines in the overlapped regions are also an indication that the trilinear interpolation process is adequate for the present purposes. Despite the coarse meshes used in the present simulations, it is correct to state that the present 3-D thin-layer Navier-Stokes calculations were able to qualitatively reproduce the expected flow features. A more detailed quantitative validation of these results is presently being undertaken and it involves the use of computational grids which are substantially finer than the ones here used, especially in the afterbody regions. Furthermore, efforts in the implementation of a simple turbulence model are also being performed, since these launch vehicle flows are clearly turbulent in actual flight. In the present work, the effect of turbulent transport has been intentionally neglected, because the effort should be seen as an evolutionary step towards the complete simulation capability.

REFERENCES

Buonomo, A.C., Strauss, D. & Azevedo, J.L.F., 1998, Axisymmetric simulations of turbulent compressible flows over aerospace vehicle, ICAS paper No. 98-2.8.3, Proceedings of the International Council of the Aeronautical Sciences, Melbourne, Australia.

Beam, R.M. & Warming, R.F., 1978, An implicit factored scheme for compressible Navier-Stokes Equations, AIAA Journal, vol. 16, pp. 393-402.

Benek, J.A., Buning, P.G. & Steger, J.L., 1985, A 3-D Chimera grid embedding technique, 7th AIAA Computational Fluid Dynamics Conference, AIAA 85-1523, Cincinnati, Ohio, USA.

Chattot, J. & Wang, J., 1998, Improved treatment of intersection bodies with the Chimera method and validation with a simple and fast flow solver, Computers & Fluid, vol. 27, pp. 721-740.

Fletcher,C.AJ., 1990, Computational techniques for fluid dynamics, 2nd Edition, Vol. II, Sydney.

Pulliam, T.H. and Steger, J. L., 1980, Implicit finite difference simulations of the three dimensional compressible flow, AIAA Journal, vol. 18, pp. 159-167.

Pulliam, T.H., 1986, Artificial dissipation models for the Euler equation, AIAA Journal, Vol. 24, No. 12, pp. 1931-1940.

Rock,S.G. & Habchi,S.D., 1998, Validation of an automated Chimera methodology for aircraft escape systems analysis, 36th AIAA Aerospace Science Meeting & Exhibit, 98-0767, Reno-NV.

Yagua, L.C.Q. , Basso, E. & Azevedo, J.L.F., 1999, Three dimensional Chimera Grid flow simulations over aerospace configurations, AIAA paper 99-3132, 17th AIAA Applied Aerodynamics Conference, Norfolk, VA, USA.

Yagua, L.C.Q. & Azevedo, J.L.F., 1999, Aplication of the Chimera for three Dimensional Compressible Flow Simulation, Proceedings of the 15th. Brazilian Congress of Mechanical Engineering – COBEM 99, Aguas de Lindoia, SP.